Rapid Communications

Combined tensor network/cluster expansion method using logic gates: Illustrated for (bi)excitons by a single-layer MoS_2 model system

Sandra C. Kuhn and Marten Richter*

Institut für Theoretische Physik, Nichtlineare Optik und Quantenelektronik, Technische Universität Berlin, Hardenbergstrasse 36, EW 7-1, D-10623 Berlin, Germany

(Received 25 July 2018; revised manuscript received 17 May 2019; published 3 June 2019)

Carriers such as electrons and holes inside the Brillouin zone of complex semiconducting materials can form bound states (excitons, biexcitons, etc.). For obtaining the corresponding eigenstates (e.g., through the Wannier or Bethe-Salpeter equation) and dynamics (e.g., cluster expansion) the number of involved electrons and holes as well as the accuracy is limited by the appearing high-dimensional tensors (i.e., wave functions or correlations). These tensors can be efficiently represented and manipulated via tensor network methods. We show how tensor networks formulated via classic logic gates can be used to treat electron-hole complexes inside the Brillouin zone. The method is illustrated for the exciton and biexciton states of a single-layer transition-metal dichalcogenide MoS_2-like model system.

DOI: 10.1103/PhysRevB.99.241301

Introduction. Semiconductor Bloch equations and cluster expansion methods have been the workhorse for optical-induced carrier and exciton dynamics in semiconductor materials for decades [1–7]. Even for the recent monolayer two-dimensional (2D) materials such as monolayer transition-metal dichalcogenides (TMDCs), these methods are still successful. However, most treatments of Coulomb bound electron-hole states were restricted to exciton states. Trion and biexciton states and beyond are seldom included [4,8–13]. If they are included, the correlations are expanded in a basis of few bound exciton, trion, or biexciton states [4,8–11,13].

Exciton states are calculated using the Wannier equation [4,8,14–16], either in real space [8,10,16,17] or in reciprocal space [14,15,18]. Often the evaluation is restricted for excitons living near high symmetrical points such as the Γ or K and K' points. In the context of *ab initio* treatments, the equivalent Bethe-Salpeter equation (BSE) is used for calculating exciton states [18–24]. On the other hand, calculations for higher-order correlated electron-hole states such as trions or biexcitons are sparse [8,10,11,13,25–29]. This Rapid Communication will illustrate a route to make bigger electron-hole complexes accessible, dynamically or for obtaining bound eigenstates.

Higher-order correlations (induced by, e.g., Coulomb, electron-phonon, or electron-photon interactions) for few level systems such as quantum dots have been successfully addressed by inductive equation of motion methods [30–32]. However, these methods are restricted to systems with few discrete levels and few discrete photon or phonon modes and cannot be applied so far to correlations with many continuous quasimomentum indices. The required memory sizes for storing the correlations scale exponentially in the number of involved particles N and polynomial in the number of involved states M ($\propto M^N$). Even small numbers of involved particles, e.g., $N = 4$ leads for a treatment of a two-dimensional Brillouin zone (BZ) (e.g., for small 30 momentum points in each dimension a two-band model yields $M = 1800$), to a hard numerical problem. So the stored data required for the simulation is the bottleneck to attack higher-order correlations. However, the naive raw data amount required to store entire movies on our computers and smartphones is at least impractical, but lossy data compression solves this issue and storing hundreds of movies on a single computer is possible. So, for treating higher-order many-particle correlations, a lossy data compression method and the ability to calculate directly on the compressed data will be the solution. Expanding the correlations in a basis (e.g., exciton [4,9], trion [10,11,25], biexciton [13,26], permutational symmetric basis [33,34]) is in principle already a first simple form of data compression, where known symmetries and properties of the problem are used for an efficient description of the system. However, for every problem a different or modified basis is required, where the reformulation and implementation of the equations is tedious and requires substantial effort. In the context of highly correlated quantum systems, tensor network methods such as matrix product states (MPS) provided a systematic and reliable way to store and manipulate quantum states of, e.g., spin chains [35–38], and also system-bath interactions [39,40]. The wave function of the spin chain is interpreted as a tensor and decomposed in a tensor network such as a MPS [also called a tensor train (TT)]. In mathematics and chemistry a new trend uses TT (or other tensor networks) to compress high-dimensional tensors regardless of whether the tensor represents an actual quantum mechanical wave function [40].

Furthermore, for solving partial differential equations in real space, quantics tensor trains (QTTs) were introduced [41–46]. QTTs do not use the spatial coordinates as indices of the tensors, but instead use their binary representation. We transfer this concept to cluster expansion and Wannier

*marten.richter@tu-berlin.de

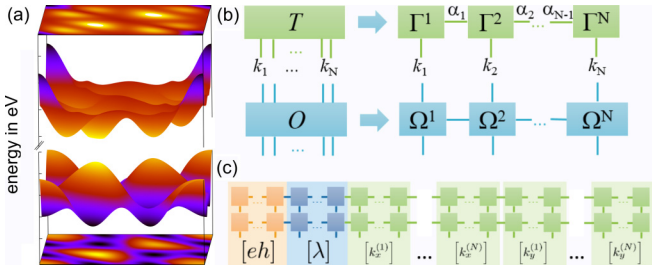

FIG. 1. (a) Valence and conduction band of MoS_2 for one spin. (b) Decomposition of a tensor into a tensor train. (c) Diagrammatic representation of the tensor train coding $S(\mathbf{k}_1^L \cdots \mathbf{k}_n^L | \mathbf{k}_1^R \cdots \mathbf{k}_m^R)$.

equations, since correlations appearing there are also tensors. We show that a binary representation of the BZ quasimomentum allows a straightforward expression of the material equations using tensor networks with binary logic gates. We focus on the calculation for a model system with a realistic numerical complexity, which describes excitons and biexcitons formed between the valence and conduction bands of the two-dimensional TMDC MoS_2 [8,13,15,27,47–52]. Currently, monolayer TMDCs such as MoS_2 are intensively researched as a new material for applications as (quantum) optical devices. In particular, very strong excitonic effects caused by the remarkably strong Coulomb interactions make monolayer TMDCs a very unique class of materials. The band structure of MoS_2 [cf. Fig. 1(a)] shows several valence and conduction band extrema, which are relevant to the formation of bound electron-hole complexes (e.g., for the exciton a ground state is formed by electrons and holes at the K or K' point). In particular, for larger electron-hole complexes such as biexcitons or trions, long-range Coulomb interactions inside the full BZ become important. A calculation of the full BZ has the advantage that all possible bound quasiparticles formed by Coulomb interactions are included, not only just the one localized at the usually investigated K and K' symmetry points.

We demonstrate that the electrons and holes complex quantities can be calculated using a very high number of grid points in the BZ. This Rapid Communication is a proof of principle that a combination of tensor network methods increases the range of problems addressable with the Wannier equation and BSE. The MoS_2 is chosen as the model system, since it is one of the most widely studied TMDCs and the tight-binding band structure is available from the literature [53,54] as a solid basis for the model system. Besides the calculation of (bi)exciton states, the concept is also extensible towards solving equations of motions in cluster expansion.

Model system. The Hamilton operator H of the model system is $H = H_0 + H_C$. The electronic band structure enters the Hamiltonian through $H_0 = \hbar \sum_{\mathbf{k}\lambda} \varepsilon_{\mathbf{k}}^{\lambda} a_{\mathbf{k}\lambda}^{\dagger} a_{\mathbf{k}\lambda}$, where $\mathbf{k}$ is the quasimomentum in BZ, and λ describes the band and spin. $\varepsilon_{\mathbf{k}}^{\lambda}$ is the band structure of the material, and for this Rapid Communication the tight-binding band structure for MoS_2 from Refs. [53,54] is used. Depending on the band $\lambda = c_\sigma, v_\sigma$ distinguishing conduction c and valence band v, with spin $\sigma = \uparrow, \downarrow$, $a_{\mathbf{k}\lambda}^{\dagger}$, $a_{\mathbf{k}\lambda}$ are the creation and annihilation operator of an electron (conduction band) or hole (valence band): $a_{\mathbf{k}\lambda_\sigma = c_\sigma}^{\dagger} = e_{\mathbf{k}\sigma}^{\dagger}$ and $a_{\mathbf{k}\lambda_\sigma = v_\sigma}^{\dagger} = h_{\mathbf{k}\sigma}^{\dagger}$. The Coulomb interaction Hamiltonian H_C reads $H_C = \sum_{\mathbf{k}_1\mathbf{k}_2\mathbf{q}\lambda_1\lambda_2} I_{\lambda_1\lambda_2}^{\mathbf{k}_1\mathbf{k}_2\mathbf{q}} a_{\mathbf{k}_1\lambda_1}^{\dagger} a_{\mathbf{k}_2\lambda_2}^{\dagger} a_{\mathbf{k}_2+\mathbf{q}\lambda_2} a_{\mathbf{k}_1 - C_{\lambda_1}^{\lambda_2}\mathbf{q}\lambda_1}$.

$C_{\lambda_1}^{\lambda_2}$ is 1, if λ_1 and λ_2 are both holes or both electrons and -1 otherwise. The prefactor $I_{\lambda_1\lambda_2}^{\mathbf{k}_1\mathbf{k}_2\mathbf{q}} = F_{\mathbf{q}}^{\mathbf{k}_1\mathbf{k}_2} V_{\mathbf{q}} C_{\lambda_1}^{\lambda_2}$ includes the Keldysh-style Coulomb potential $V_{\mathbf{q}}$ [15,55] and the tight-binding (TB) coefficients $c_{\mathbf{k}n_1}$ inside $F_{\mathbf{q}}^{\mathbf{k}_1\mathbf{k}_2} = \sum_{n_1,n_2} c_{\mathbf{k}_1 n_1}^{*} c_{\mathbf{k}_2 n_2}^{*} c_{\mathbf{k}_2+\mathbf{q}n_2} c_{\mathbf{k}_1 - C_{\lambda_1}^{\lambda_2}\mathbf{q}n_1}$. The Coulomb potential $V_{\mathbf{q}}$ is calculated for MoS_2 on a silica substrate (air/silica interface). The model system is slightly simplified (no exchange coupling term), since this work is focused on the method (more accurate treatments are subject to future studies).

We introduce the multi-index $\mathbf{k} = \{\mathbf{k}\lambda\}$, where λ is only written explicitly, if needed. The correlations describing the system are $\langle a_{\mathbf{k}_1^L}^{\dagger} \cdots a_{\mathbf{k}_n^L}^{\dagger} a_{\mathbf{k}_m^R} \cdots a_{\mathbf{k}_1^R} \rangle =: S(\mathbf{k}_1^L \cdots \mathbf{k}_n^L | \mathbf{k}_1^R \cdots \mathbf{k}_m^R)$. Using Heisenberg equations of motion $\partial_t \langle O \rangle = i/\hbar \langle [H, O]_- \rangle$, we arrive at an equation for S,

$$\begin{aligned}\partial_t S\big(\mathbf{k}_1^L \cdots \mathbf{k}_n^L | \mathbf{k}_1^R \cdots \mathbf{k}_m^R\big) = {} & i \sum_{j=1}^{n} \varepsilon_{\mathbf{k}_j^L} S(\cdots|\cdots) - 2i \sum_{j\mathbf{k}\mathbf{q}} I_{\lambda_j^R \lambda}^{\mathbf{k}_j^R \mathbf{k}\mathbf{q}} S\big(\cdots \mathbf{k}_n^L \{\mathbf{k}+\mathbf{q}\} | \cdots \big\{\mathbf{k}_j^R - C_{\lambda_j^R}^{\lambda} \mathbf{q}\big\} \cdots \mathbf{k}_m^R \mathbf{k}\big) \\ & - 2i \sum_{i<j\mathbf{q}} I_{\lambda_j^R \lambda_i^R}^{\mathbf{k}_j^R \mathbf{k}_i^R \mathbf{q}} S\big(\cdots \big| \cdots \big\{\mathbf{k}_j^R - C_{\lambda_j^R}^{\lambda} \mathbf{q}\big\} \cdots \big\{\mathbf{k}_i^R + \mathbf{q}\big\} \cdots\big) - \{L \leftrightarrow R, n \leftrightarrow m\}. \end{aligned} \tag{1}$$

On the right-hand side (rhs) only the changes in the indices of $S(\cdots|\cdots)$ compared to the left-hand side (lhs) are denoted. Note, some terms on the rhs change the number of indices of $S(\cdots|\cdots)$ compared to the lhs. Equation (1) creates the usual infinite hierarchy of correlations, which is usually driven by electron-light interaction terms, not included here. Examples of higher-order correlations include important spectroscopic contributions such as $S(\mathbf{k}_1\mathbf{k}_2\mathbf{k}_3|\mathbf{k}_4)$ (contains density-assisted polarizations leading to excitation-induced dephasing), $S(\mathbf{k}_1\mathbf{k}_2\mathbf{k}_3\mathbf{k}_4|)$ (contains biexcitonic coherences), or $S(\mathbf{k}_1\mathbf{k}_2\mathbf{k}_3\mathbf{k}_4|\mathbf{k}_5\mathbf{k}_6)$ (contains single-exciton to biexciton correlations). These higher-order tensors $S(\cdots|\cdots)$ impose a high numerical burden that tensor network methods will lift. While future calculations of the quantum dynamics using Eq. (1) and the tensor network approach are possible, we focus here on the calculation of many-particle eigenstates, i.e., eigenstates for excitons, biexcitons, etc. As in the calculation of the Wannier equation [14], we take the homogeneous part of Eq. (1) and convert the equation to an eigenproblem with eigenenergies E for the respective many-particle

complexes,

$$iE\,S\big(\mathbf{k}_1^L\cdots\mathbf{k}_n^L|\mathbf{k}_1^R\cdots\mathbf{k}_m^R\big)=i\sum_{j=1}^{n}\varepsilon_{\mathbf{k}_j^L}S(\cdots|\cdots)-2i\sum_{i<j\mathbf{q}}I^{\mathbf{k}_j^R\mathbf{k}_i^R\mathbf{q}}_{\lambda_j^R\lambda_i^R}S\big(\cdots\big|\cdots\big\{\mathbf{k}_j^R-C^{\lambda}_{\lambda_j^R}\mathbf{q}\big\}\cdots\big\{\mathbf{k}_i^R+\mathbf{q}\big\}\cdots\big)-\{L\leftrightarrow R,n\leftrightarrow m\}. \tag{2}$$

Then, for $S(|\mathbf{k}_1\cdots\mathbf{k}_N)$, Eq. (2) actually has the same form as the Hermitian conjugate of the Schrödinger equation of $\Psi_{\mathbf{k}_1\cdots\mathbf{k}_N}=a^\dagger_{\mathbf{k}_1}\cdots a^\dagger_{\mathbf{k}_N}|\Psi_0\rangle$, which describes the bound electron-hole carriers created out of the neutral ground state $|\Psi_0\rangle$ (without prior doping or optical excitation) of the system. Therefore, for $S(|\mathbf{k}_1\mathbf{k}_2)$, Eq. (2) corresponds to the Wannier equation, the eigenstate problem for excitons (bound electron-hole pairs) [14] in reciprocal space, and is equivalent to a BSE [4,21,28]. Remember, $\langle a_{\mathbf{k}v_{\sigma_1}}a_{\mathbf{k}c_{\sigma_2}}\rangle$ is part of $S(|\mathbf{k}_1\mathbf{k}_2)$ and is an electron-hole coherence $\langle h_{\mathbf{k}\sigma_1}e_{\mathbf{k}\sigma_2}\rangle$. Furthermore, for $S(|\mathbf{k}_1\mathbf{k}_2\mathbf{k}_3\mathbf{k}_4)$, Eq. (2) is the generalization to biexcitons, i.e., bound complexes from two electrons and two holes. In this Rapid Communication, we will focus on excitons and biexcitons.

Tensor network methods. In principle, $S(\mathbf{k}_1^L\cdots\mathbf{k}_n^L|\mathbf{k}_1^R\cdots\mathbf{k}_m^R)$ is a tensor with indices $\mathbf{k}_1^L,\ldots,\mathbf{k}_n^L,\mathbf{k}_1^R,\ldots,\mathbf{k}_m^R$ and rank $n+m$. If we assume $g=1000$ grid points for the BZ (which is probably too small), the memory requirement is $g^{n+m}=1000^{n+m}$, so that already for very small m and n the memory exceeds the feasible and possible range. Reference [56] showed that every tensor $T_{k_1,\ldots,k_N}$ can be approximated as MPS (in mathematics, TT) in the form $T_{k_1,\ldots,k_n}=\sum_{\alpha_1,\ldots,\alpha_{n-1}}\Gamma^{1,k_1}_{\alpha_1}\Gamma^{2,k_2}_{\alpha_1\alpha_2}\Gamma^{3,k_3}_{\alpha_2\alpha_3}\cdots\Gamma^{n,k_n}_{\alpha_{n-1}}$. The tensors $\Gamma^{n,k}_{\alpha\alpha'}$ have a maximum of gD^2 elements, if D is the maximum number of α_i (link dimension). If the relevant information of the tensor can be represented with small D, the overall memory size reduces from exponential scaling g^{n+m} to linear scaling $(n+m)gD^2$, making higher-dimensional tensors accessible [37,56–58]. In the following, we will use a diagrammatic notation for tensors [37,57,58]: The tensor is represented by a rectangle and indices are denoted as lines [cf. Fig. 1(b)]. If the two indices of a tensor are contracted (summed), the lines are connected, so that the decomposition of the tensor $T_{k_1,\ldots,k_n}$ into $\Gamma^{n,k}_{\alpha\alpha'}$ is represented by the diagram in Fig. 1(b). Tensors are mathematically vectors, and simple vector operations such as adding, taking the norm, and scalar multiplication can be carried out directly on the MPS form without reconstructing the full tensor [57,58]. Linear operators $O_{k_1,\ldots,k_n,k'_1,\ldots,k'_n}$ acting on tensors represented as MPS can be described as matrix product operators (MPOs), which can be applied efficiently on MPS [see Fig. 1(b) and Refs. [57–59]].

Representing $S(\mathbf{k}_1^L\cdots\mathbf{k}_n^L|\mathbf{k}_1^R\cdots\mathbf{k}_m^R)$ directly as MPS is not a good idea, since the dimension g (the number of grid points) of $\mathbf{k}$ is very high. In Refs. [41–45] QTTs were introduced to solve this problem, also in the context of BSEs [46]. For a QTT the tensor indices are not used for the decomposition, but the bits of a binary representation of the indices resulting in a $(n+m)\log(g)D^2$ scaling of the memory requirement. For a binary representation of the 2D BZ, the quasimomentum is written as $\mathbf{k}=1/2^N\sum_{i=1}^{N}(k_x^{(i)}\mathbf{b}_x+k_y^{(i)}\mathbf{b}_y)2^i$ with the number of bits N and the basis vectors $\mathbf{b}_{x/y}$ of the BZ and bits $k_{x/y}^{(i)}=0,1$. Furthermore, the band index λ contains one bit *eh* for distinguishing valence and conduction bands and one bit for the spin *s*. The bit representation is very suitable for the interaction terms, since relations such as quasimomentum conservation including umklapp processes can be represented by binary logic gates inside tensor networks. Most binary logic operations between two $\mathbf{k}$'s connect bits from the same digit, or adjacent digits. Sorting the bit indices for the QTT/MPS decomposition by binary digits results in more efficient tensor networks. Therefore, the bits to describe the indices $\mathbf{k}_i^{L/R}$ of the tensor $S(\mathbf{k}_1^L\cdots\mathbf{k}_n^L|\mathbf{k}_1^R\cdots\mathbf{k}_m^R)$ are sorted as $([eh],[\lambda],[k_x^{(1)}],\ldots,[k_x^{(N)}],[k_y^{(1)}],\ldots,[k_y^{(N)}])$, where $[\cdot]$ represents a group of bits: $[\Lambda]=\Lambda_1^L,\ldots,\Lambda_n^L,\Lambda_m^R,\ldots\Lambda_1^R$ [cf. Fig. 1(c)]. After defining the QTT decomposition, the MPOs are built from tensor networks for the rhs terms of Eq. (2).

We start with the homogeneous energy term $-i\varepsilon_{\mathbf{k}_j^R}S(\cdots|\cdots\mathbf{k}_j^R\cdots)$, where $S(\cdots|\cdots\mathbf{k}_j^R\cdots)$ is the MPS, on which a MPO will act [see Fig. 1(c)]. We can rewrite the term as $-i\sum_{\mathbf{k}'^R_j\mathbf{k}''^R_j}\delta_{\mathbf{k}_j^R\mathbf{k}'^R_j\mathbf{k}''^R_j}\varepsilon_{\mathbf{k}'^R_j}S(\cdots|\cdots\mathbf{k}''^R_j\cdots)$, where $\delta_{\mathbf{k}_j^R\mathbf{k}'^R_j\mathbf{k}''^R_j}$ factorizes into $\prod_i\delta_{k^{(i)R}_{mj}k'^{(i)R}_{mj}k''^{(i)R}_{mj}}$ for every bit of $\mathbf{k}_j^R$ including band and spin bits. Furthermore, $\varepsilon_{\mathbf{k}_j^R}$ is converted into a QTT ε with the same bit ordering. The tensor network in Fig. 2(a) depicts the MPO of the homogeneous energy

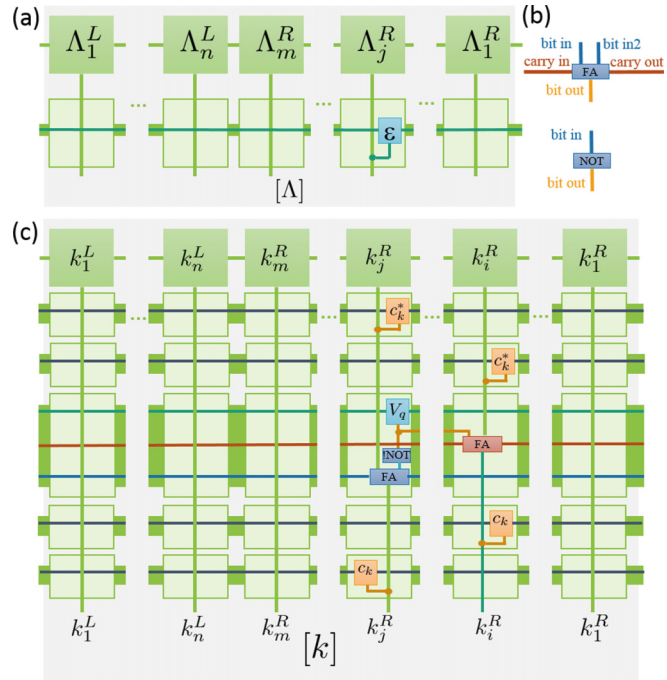

FIG. 2. (a) TN representing the homogeneous part of Eq. (2), (b) full adder (FA), and negation (NOT) logical circuits. (c) TN representing the Coulomb term of Eq. (2) (only *k* part).

term. The δ-bit tensor is represented by a dot in Fig. 2 and connects the initial MPS bit index with the bit index of $\varepsilon_{\mathbf{k}_j^R}$ and the final bit index. For every tensor network construction, the key design principle is to ensure the correct flow of index information from the initial MPS [$S(\cdots|\cdots)$ on the rhs] to the term prefactors inside the MPO to the final MPS indices [$S(\cdots|\cdots)$ on the lhs]. In the TN in Fig. 2(a) the connections and junction ensure that the same indices of the initial tensor on the rhs of Eq. (2), the energy tensor $\varepsilon_{\mathbf{k}_j^R}$ and the tensor on the lhs are connected.

Constructing the TN for the Coulomb term $-2i\sum_{i<j\mathbf{q}} I^{\mathbf{k}_j^R\mathbf{k}_i^R\mathbf{q}}_{\lambda_j^R\lambda_i^R} S(\cdots|\cdots\{\mathbf{k}_j^R - C^{\lambda}_{\lambda_j^R}\mathbf{q}\}\cdots\{\mathbf{k}_i^R+\mathbf{q}\}\cdots)$ is more involved and will require five MPOs, which are subsequently compressed to a single MPO. $\mathbf{q}$ has positive and negative components, and negative numbers are encoded using two's complement representation for binary negative integers [60], which matches nicely the periodic properties of the BZ. (A negative $\mathbf{q}$ is represented by a positive $\mathbf{q}+\mathbf{G}$ inside the BZ with suitable $\mathbf{G}$.) For the correct flow of information the TN has to connect the bit indices for $\mathbf{k}_i^R$, $\mathbf{k}_j^R$, $\mathbf{k}_i^R-\mathbf{q}$, $\mathbf{k}_j^R + C^{\lambda}_{\lambda_j^R}\mathbf{q}$, and $\mathbf{q}$ with $C^{\lambda}_{\lambda_j^R} = \pm 1$. Tensors representing binary logic gates achieve this: A set of full adders [60] calculates $\mathbf{k}_i^R-\mathbf{q}$ and $\mathbf{k}_j^R + C^{\lambda}_{\lambda_j^R}\mathbf{q}$ from $\mathbf{k}_i^R$, $\mathbf{k}_j^R$, and $\mathbf{q}$. For the case $C^{\lambda}_{\lambda_j^R} = -1$ additional NOT circuits convert $\mathbf{q}$ to a negative input in two's complement representation for the full adder. The corresponding TN is shown in Fig. 2(c); the application of $V_{\mathbf{q}}$ and calculation of the indices is handled by the MPO in the middle of the set of five MPOs. Here, the full adders combine the $\mathbf{k}$ indices and the $\mathbf{q}$ indices of $V_{\mathbf{q}}$ for every bit of the binary representation. In addition, carry bits connect the full adder for different bit digits. In Fig. 2(c) the prefactor $F_{\mathbf{q}}^{\mathbf{k}_j^R\mathbf{k}_i^R}$ is handled by the four outer MPOs. To include it, the MPO from Fig. 2 is combined with two MPOs representing $c_{\mathbf{k}_2+\mathbf{q}n_2}$, $c_{\mathbf{k}_1-C^{\lambda_2}_{\lambda_1}\mathbf{q}n_1}$ before its application and two MPOs representing $c^*_{\mathbf{k}_1 n_1}$, $c^*_{\mathbf{k}_2 n_2}$ after its application. (The Supplemental Material [61] includes a more extensive discussion.)

We use the ITensor C++ library (patched version 2.1.0) for the calculation of all tensor operations [62]. The rhs of Eq. (2) is calculated through the TN brought in the form of successive applied MPOs, which are compressed using a fitApply algorithm. In order to solve Eq. (2) and to determine the respective exciton and biexciton eigenenergies and wave functions, we first use a density matrix renormalization group (DMRG) algorithm [58,63] which is capable of obtaining the eigenvalues and eigenvectors (MPS) of a MPO. We use a modified DMRG algorithm based on the ITensor DMRG [62] implementation for adding multiple MPOs and for the calculation of higher-energy eigenvectors. For the DMRG algorithm the successive applied set of MPOs (cf. Fig. 2) has to be merged into a single MPO, however, the resulting MPO requires a very high link dimension and we could not achieve converged results. Using imaginary time propagation [57] for the final propagation resulted in converged results, since here a merger of the subsequent applied MPOs is not necessary. (See the convergence analysis in the Supplemental Material [61]) To obtain the eigenstates, Eq. (2) is solved for the exciton $S(\mathbf{k}_1^L\mathbf{k}_2^L|)$ and

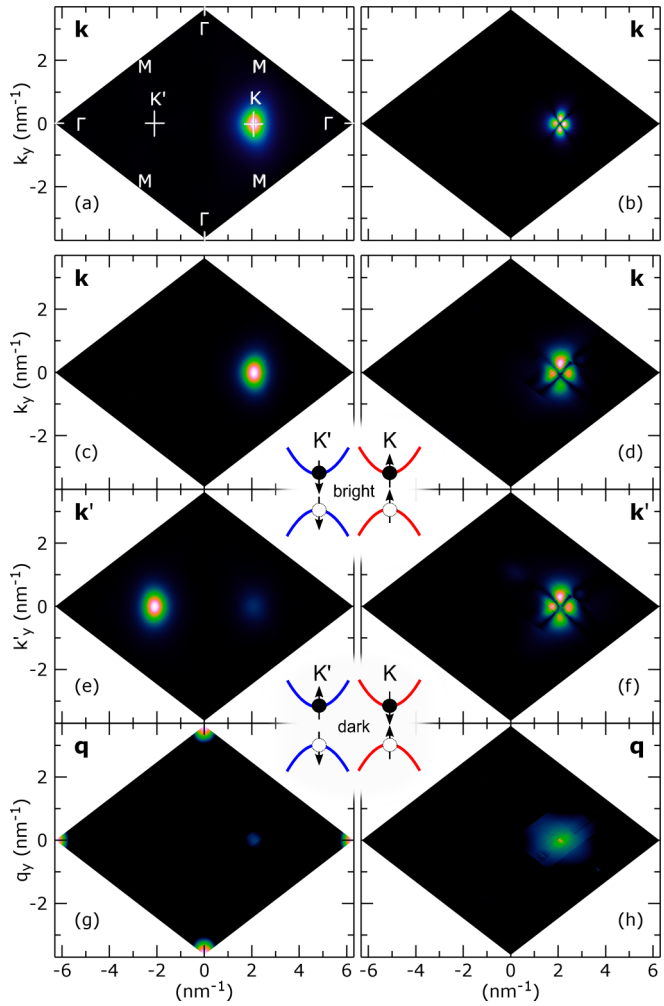

FIG. 3. Selected exciton and biexciton wave functions in BZ: (a) Bright A exciton with parallel spin up and (b) dark $3d$ exciton with antiparallel spin localized at the K valley. (c), (e), and (g) Bright biexciton formed from two bright A excitons and (d), (f), and (h) dark biexciton formed from two dark $3d$ excitons. The plotted variable is depicted in the corner. (g) and (h) are plotted using a logarithmic color scale. (a), (c), (e), and (g) are converged results using imaginary time propagation and while (b), (d), (f), and (h) use DMRG and show the potential of the method without achieving convergence.

biexciton $S(\mathbf{k}_1^L\mathbf{k}_2^L\mathbf{k}_3^L\mathbf{k}_4^L|)$ coherences/wave function on a full 1024×1024 grid for every $\mathbf{k}$ vector inside the full BZ. To address optical excitability states, we focus on (bi)exciton states with zero overall momentum $\langle a^\dagger_{\mathbf{k}v_{\sigma_1}} a^\dagger_{\mathbf{k}c_{\sigma_2}}\rangle = \langle h^\dagger_{\mathbf{k}\sigma_1} e^\dagger_{\mathbf{k}\sigma_2}\rangle$ and $\langle a^\dagger_{\mathbf{k}v_{\sigma_1}} a^\dagger_{\mathbf{k}+\mathbf{q}c_{\sigma_2}} a^\dagger_{\mathbf{k}'+\mathbf{q}v_{\sigma_3}} a^\dagger_{\mathbf{k}'c_{\sigma_4}}\rangle = \langle h^\dagger_{\mathbf{k}\sigma_1} e^\dagger_{\mathbf{k}+\mathbf{q}\sigma_2} h^\dagger_{\mathbf{k}'+\mathbf{q}\sigma_3} e^\dagger_{\mathbf{k}'\sigma_4}\rangle$, and the TN constructing this coherence from $S(\mathbf{k}_1^L\mathbf{k}_2^L\mathbf{k}_3^L\mathbf{k}_4^L|)$ is given in the Supplemental Material.

We obtain the bound, bright A exciton at 1.769 eV compared to a band gap of 2.124 eV at the K point, reproducing Ref. [54], whose band structure [53,54] is used in the model system, here. As an example from the exciton states, Fig. 3(a) shows the A exciton wave function (1.769 eV) for a parallel spin-up configuration localized at the K valley. The biexciton coherence with zero center-of-mass momentum

$\langle a^\dagger_{\mathbf{k}v_{\sigma_1}} a^\dagger_{\mathbf{k}+\mathbf{q}c_{\sigma_2}} a^\dagger_{\mathbf{k}'+\mathbf{q}v_{\sigma_3}} a^\dagger_{\mathbf{k}'c_{\sigma_4}} \rangle$ depends on the three momenta $\mathbf{k}$, $\mathbf{k}'$, and $\mathbf{q}$. To characterize the six-dimensional wave function, we sum over two momenta (e.g., $\mathbf{k}'$ and $\mathbf{q}$) while plotting over the third (e.g., over $\mathbf{k}$) in the BZ. Figures 3(c)–3(h) show two example biexciton states: Two A excitons, one electron-hole pair with parallel spin up located at the K valley [Fig. 3(c)] and another with parallel spin down at the K' valley [Fig. 3(e)], constitute a bright biexciton [note $\mathbf{q} \approx \mathbf{0}$, Fig. 3(g)] with an energy of 3.518 eV (20 meV binding energy; cf. Refs. [47,51]).

Furthermore, in principle, the approach allows also to access higher-energy bound biexciton states (bright or dark). Figures 3(d), 3(f), and 3(h) show as an example a biexciton composed from two dark $3d$ excitons with antiparallel electron-hole spin calculated using DMRG [see the wave function depicted in Fig. 3(b); cf. Ref. [64]]. However, using DMRG, the ordering of calculated higher excited states was highly parameter dependent and we could not achieve convergence, showing the need for modified DMRG types for excited states [65–67] and successive applied MPOs. Besides the example exciton and biexciton states, the framework allows us to determine many higher-energy bound electron-holes states, in principle, also for other correlated electron and hole quasiparticles such as trions.

In conclusion, the combination of tensor networks, cluster expansion, and logic gates on the Brillouin zone allows us to easily access bound electron-hole quasiparticles with little numerical cost and high precision. We demonstrated our method on the example of excitonic and biexcitonic states in MoS_2 on a silicone substrate. The exciton energies fit well with the results presented in Ref. [54], whose band structure is used in our model. The biexciton binding energy is in the same order of magnitude as reported in the literature [47,51]. Future studies in this framework will provide systematic investigations of the bound electron-hole complexes and extend the numerical technique to quantum dynamics.

Acknowledgments. We gratefully acknowledge support from the Deutsche Forschungsgemeinschaft (DFG) through SFB 787 B1 (project no. 43659573). We thank E. Miles Stoudenmire for helpful tips and fast patches of the ITensor library. We also acknowledge useful discussions with Jonathan Schwarz.

[1] M. Lindberg and S. W. Koch, Phys. Rev. B **38**, 3342 (1988).
[2] S. Butscher, J. Förstner, I. Waldmüller, and A. Knorr, Phys. Rev. B **72**, 045314 (2005).
[3] D. Reiter, M. Glanemann, V. M. Axt, and T. Kuhn, Phys. Rev. B **75**, 205327 (2007).
[4] R. Schmidt, G. Berghäuser, R. Schneider, M. Selig, P. Tonndorf, E. Malic, A. Knorr, S. Michaelis de Vasconcellos, and R. Bratschitsch, Nano Lett. **16**, 2945 (2016).
[5] S. Chatterjee, C. Ell, S. Mosor, G. Khitrova, H. M. Gibbs, W. Hoyer, M. Kira, S. W. Koch, J. P. Prineas, and H. Stolz, Phys. Rev. Lett. **92**, 067402 (2004).
[6] T. Winzer, A. Knorr, and E. Malic, Nano Lett. **10**, 4839 (2010).
[7] L. Meckbach, T. Stroucken, and S. W. Koch, Phys. Rev. B **97**, 035425 (2018).
[8] E. Mostaani, M. Szyniszewski, C. H. Price, R. Maezono, M. Danovich, R. J. Hunt, N. D. Drummond, and V. I. Fal'ko, Phys. Rev. B **96**, 075431 (2017).
[9] T. Östreich, K. Schönhammer, and L. J. Sham, Phys. Rev. B **58**, 12920 (1998).
[10] A. Esser, E. Runge, R. Zimmermann, and W. Langbein, Phys. Status Solidi A **178**, 489 (2000).
[11] A. Esser, R. Zimmermann, and E. Runge, Phys. Status Solidi B **227**, 317 (2001).
[12] A. E. Almand-Hunter, H. Li, S. T. Cundiff, M. Mootz, M. Kira, and S. W. Koch, Nature (London) **506**, 471 (2014).
[13] A. Steinhoff, M. Florian, A. Singh, K. Tran, M. Kolarczik, S. Helmrich, A. W. Achtstein, U. Woggon, N. Owschimikow, F. Jahnke *et al.*, Nat. Phys. **14**, 1199 (2018).
[14] H. Haug and S. W. Koch, *Quantum Theory of the Optical and Electronic Properties of Semiconductors*, 5th ed. (World Scientific, Singapore, 2009).
[15] G. Berghäuser and E. Malic, Phys. Rev. B **89**, 125309 (2014).
[16] M. Richter, Phys. Rev. Mater. **1**, 016001 (2017).
[17] R. Singh, M. Richter, G. Moody, M. E. Siemens, H. Li, and S. T. Cundiff, Phys. Rev. B **95**, 235307 (2017).
[18] F. Hüser, T. Olsen, and K. S. Thygesen, Phys. Rev. B **88**, 245309 (2013).
[19] P. Rinke, A. Schleife, E. Kioupakis, A. Janotti, C. Rödl, F. Bechstedt, M. Scheffler, and C. G. Van de Walle, Phys. Rev. Lett. **108**, 126404 (2012).
[20] P. Cudazzo, C. Attaccalite, I. V. Tokatly, and A. Rubio, Phys. Rev. Lett. **104**, 226804 (2010).
[21] D. Y. Qiu, F. H. da Jornada, and S. G. Louie, Phys. Rev. Lett. **111**, 216805 (2013).
[22] R. Laskowski, N. E. Christensen, G. Santi, and C. Ambrosch-Draxl, Phys. Rev. B **72**, 035204 (2005).
[23] D. Y. Qiu, T. Cao, and S. G. Louie, Phys. Rev. Lett. **115**, 176801 (2015).
[24] E. Torun, H. P. C. Miranda, A. Molina-Sánchez, and L. Wirtz, Phys. Rev. B **97**, 245427 (2018).
[25] B. Stébé, G. Munschy, L. Stauffer, F. Dujardin, and J. Murat, Phys. Rev. B **56**, 12454 (1997).
[26] O. Mayrock, H.-J. Wünsche, F. Henneberger, C. Riva, V. A. Schweigert, and F. M. Peeters, Phys. Rev. B **60**, 5582 (1999).
[27] A. Singh, G. Moody, K. Tran, M. E. Scott, V. Overbeck, G. Berghäuser, J. Schaibley, E. J. Seifert, D. Pleskot, N. M. Gabor *et al.*, Phys. Rev. B **93**, 041401(R) (2016).
[28] M. Florian, M. Hartmann, A. Steinhoff, J. Klein, A. W. Holleitner, J. J. Finley, T. O. Wehling, M. Kaniber, and C. Gies, Nano Lett. **18**, 2725 (2018).
[29] M. Drüppel, T. Deilmann, P. Krüger, and M. Rohlfing, Nat. Commun. **8**, 2117 (2017).
[30] J. Kabuss, A. Carmele, M. Richter, and A. Knorr, Phys. Rev. B **84**, 125324 (2011).
[31] A. Carmele, M. Richter, W. W. Chow, and A. Knorr, Phys. Rev. Lett. **104**, 156801 (2010).
[32] H. A. M. Leymann, A. Foerster, and J. Wiersig, Phys. Rev. B **89**, 085308 (2014).
[33] M. Gegg and M. Richter, New J. Phys. **18**, 043037 (2016).
[34] M. Gegg and M. Richter, Sci. Rep. **7**, 16304 (2017).

[35] F. Verstraete and J. I. Cirac, Phys. Rev. B **73**, 094423 (2006).
[36] G. Vidal, Phys. Rev. Lett. **98**, 070201 (2007).
[37] J. Cirac, D. Prez-Garca, N. Schuch, and F. Verstraete, Ann. Phys. **378**, 100 (2017).
[38] S. R. Clark, J. Prior, M. J. Hartmann, D. Jaksch, and M. B. Plenio, New J. Phys. **12**, 025005 (2010).
[39] A. H. Werner, D. Jaschke, P. Silvi, M. Kliesch, T. Calarco, J. Eisert, and S. Montangero, Phys. Rev. Lett. **116**, 237201 (2016).
[40] Q. Shi, Y. Xu, Y. Yan, and M. Xu, J. Chem. Phys. **148**, 174102 (2018).
[41] I. V. Oseledets, Doklady Mathematics **80**, 653 (2009).
[42] I. V. Oseledets, SIAM J. Matrix Anal. Appl. **31**, 2130 (2010).
[43] B. N. Khoromskij, Constr. Approx. **34**, 257 (2011).
[44] V. A. Kazeev and B. N. Khoromskij, SIAM J. Matrix Anal. Appl. **33**, 742 (2012).
[45] V. Khoromskaia and B. N. Khoromskij, Phys. Chem. Chem. Phys. **17**, 31491 (2015).
[46] P. Benner, S. Dolgov, V. Khoromskaia, and B. N. Khoromskij, J. Comput. Phys. **334**, 221 (2017).
[47] K. Hao, J. F. Specht, P. Nagler, L. Xu, K. Tran, A. Singh, C. K. Dass, C. Schüller, T. Korn, M. Richter *et al.*, Nat. Commun. **8**, 15552 (2017).
[48] X.-X. Zhang, Y. You, S. Y. F. Zhao, and T. F. Heinz, Phys. Rev. Lett. **115**, 257403 (2015).
[49] E. J. Sie, A. J. Frenzel, Y.-H. Lee, J. Kong, and N. Gedik, Phys. Rev. B **92**, 125417 (2015).
[50] T. Olsen, S. Latini, F. Rasmussen, and K. S. Thygesen, Phys. Rev. Lett. **116**, 056401 (2016).
[51] M. Szyniszewski, E. Mostaani, N. D. Drummond, and V. I. Fal'ko, Phys. Rev. B **95**, 081301(R) (2017).
[52] M. Selig, G. Berghäuser, M. Richter, R. Bratschitsch, A. Knorr, and E. Malic, 2D Mater. **5**, 035017 (2018).
[53] E. Ridolfi, D. Le, T. Rahman, E. Mucciolo, and C. Lewenkopf, J. Phys.: Condens. Matter **27**, 365501 (2015).
[54] E. Ridolfi, C. H. Lewenkopf, and V. M. Pereira, Phys. Rev. B **97**, 205409 (2018).
[55] T. C. Berkelbach, M. S. Hybertsen, and D. R. Reichman, Phys. Rev. B **88**, 045318 (2013).
[56] G. Vidal, Phys. Rev. Lett. **91**, 147902 (2003).
[57] R. Orús, Ann. Phys. **349**, 117 (2014).
[58] U. Schollwöck, Ann. Phys. **326**, 96 (2011).
[59] G. Vidal, Phys. Rev. Lett. **93**, 040502 (2004).
[60] U. Tietze, C. Schenk, and E. Gamm, *Electronic Circuits: Handbook for Design and Application* (Springer, Berlin, 2015).
[61] See Supplemental Material at http://link.aps.org/supplemental/10.1103/PhysRevB.99.241301 for a full representation of the matrix product operators (MPOs) used, with standard logical circuits and a convergence analysis.
[62] E. M. Stoudenmire and S. R. White, ITensor C++ library, http://itensor.org/.
[63] S. R. White, Phys. Rev. Lett. **69**, 2863 (1992).
[64] D. Y. Qiu, F. H. da Jornada, and S. G. Louie, Phys. Rev. B **93**, 235435 (2016).
[65] S. P. Lim and D. N. Sheng, Phys. Rev. B **94**, 045111 (2016).
[66] X. Yu, D. Pekker, and B. K. Clark, Phys. Rev. Lett. **118**, 017201 (2017).
[67] V. Khemani, F. Pollmann, and S. L. Sondhi, Phys. Rev. Lett. **116**, 247204 (2016).